Supporting Information
Photonic Properties and Applications of Cellulose Nanocrystal Films with Planar Anchoring

*Partha Saha and Virginia A. Davis**
Department of Chemical Engineering, Auburn University,
Auburn University, AL 36849, United States
*Email: davisva@auburn.edu

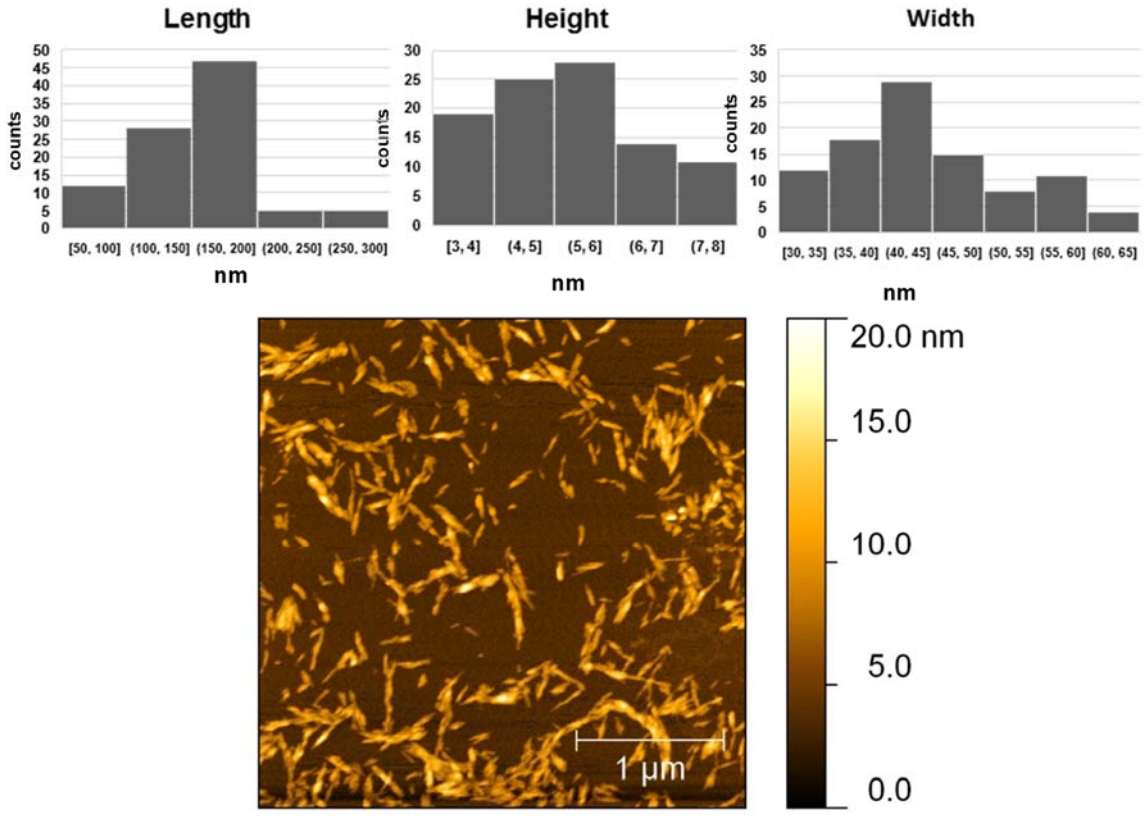

Figure S1. AFM measurements showing cellulose nanocrystals length, height, and width distributions. Width measurements are based on results after using Gwyddion's blind tip estimation.

Figures S2 – S9 show CNC films dried on a microscope glass slide using the 2.0 wt. % (1.3 vol. %) isotropic, 6.5 wt. % (4.2 vol. %) biphasic and 8.0 wt. % (5.1 vol. %) liquid crystalline (8.0 wt. %) dispersions under different conditions. Reflected cross-polarized images of regions near the film center and near the edge (approximately along the centerline) are included for the following experiments:

- **Figure S2**: 1 surface, air drying, no shear
- **Figure S3**: 1 surface, air drying, 60 rpm orbital shear
- **Figure S4**: 1 surface, humid/slow drying, no shear
- **Figure S5**: 1 surface, humid/slow drying, 60 rpm orbital shear
- **Figure S6**: 2 surfaces, air drying, no shear
- **Figure S7**: 2 surfaces, air drying, 60 rpm orbital shear
- **Figure S8**: 2 surfaces, humid/slow drying, no shear
- **Figure S9**: 2 surface, humid/slow drying, 60 rpm orbital shear

These images support the images and results discussed in the main manuscript:

- The biphasic dispersions resulted into more uniform planar orientation with any combination of the factors as reported on the manuscript.
- Air drying (with all possible variation of the parameters) results in horizontal helix (homeotropic) ordering. The strong capillary forces can even unwind the cholesteric microstructures, particularly at the edge of the films.
- The slower drying in a humid environment resulted in more uniform microstructures.
- The marked difference between CNC films made from isotropic dispersions in humid environment with and without orbital shear, indicates the significant effect of the weak orbital shear on facilitating planar ordering (**Figure S4A, D** compared to **Figure S5A, D**).
- The effect of the coverslip (second anchoring surface) was more apparent for biphasic dispersions. Attempts to dry isotropic and biphasic dispersions at rest resulted in the dispersions being squeezed out by the weight of the coverslip.
- Drying biphasic CNC dispersions with surface anchoring, slow drying, and 60 rpm orbital shear resulted in the largest planar textures.

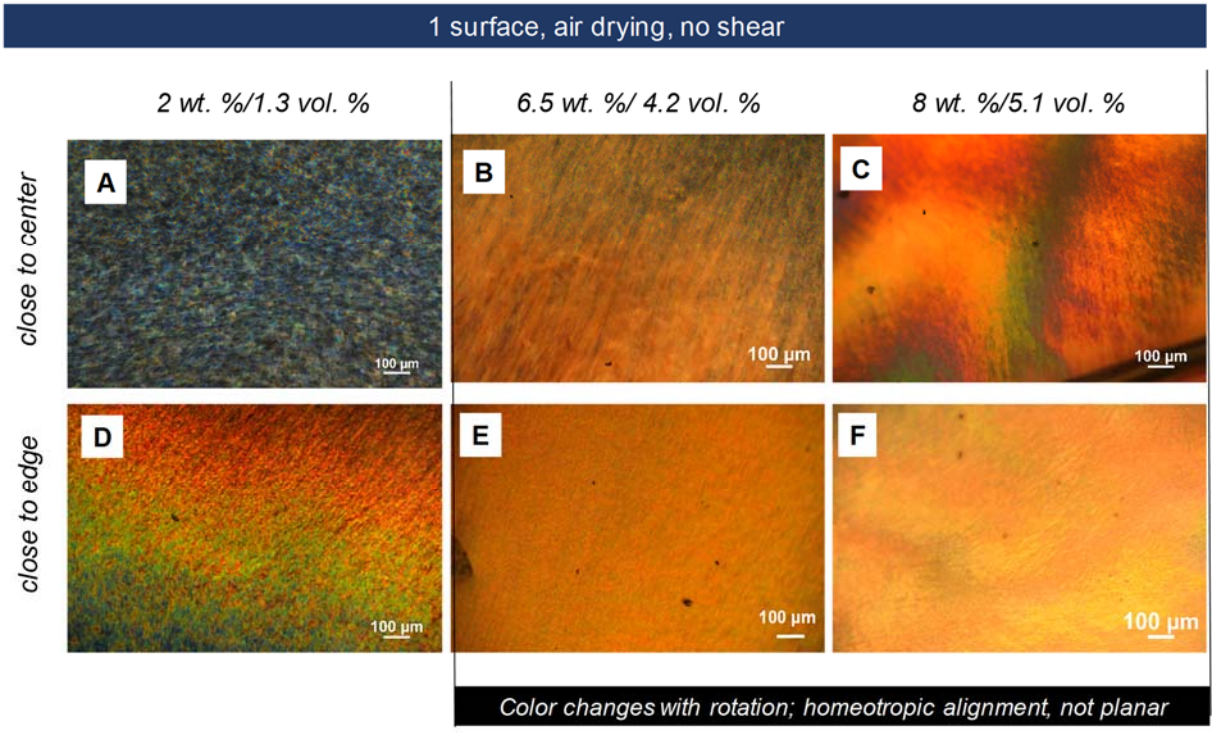

Figure S2. Cross-polarized reflected microscopic images showing CNC films made from isotropic (2.0 wt. %), biphasic (6.5 wt. %), and liquid crystalline (8.0 wt. %) using no coverslip, no shear, and air drying. A), B), C) close to the center and D), E), F) close to the edge of the films.

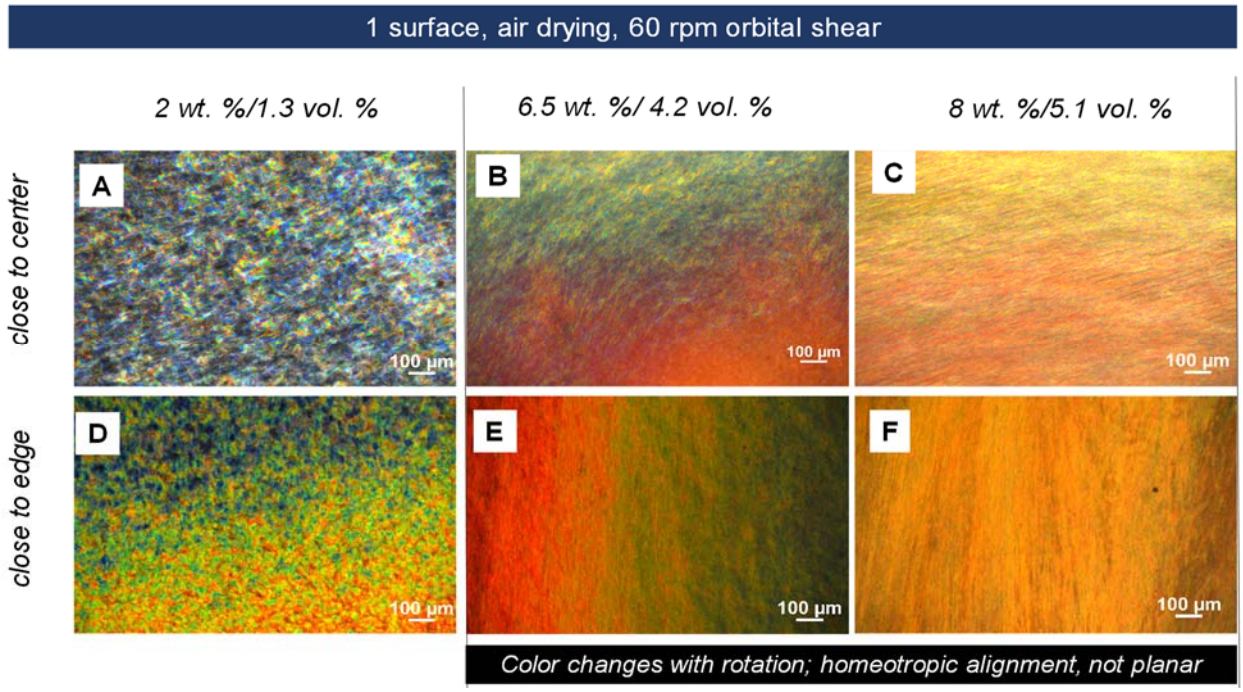

Figure S3. Cross-polarized reflected microscopic images showing CNC films made from isotropic (2 wt. %), biphasic (6.5 wt. %), and liquid crystalline (8 wt. %) using no coverslip, 60 rpm shear, and air drying. A), B), C) close to the center and D), E), F) close to the edge of the films.

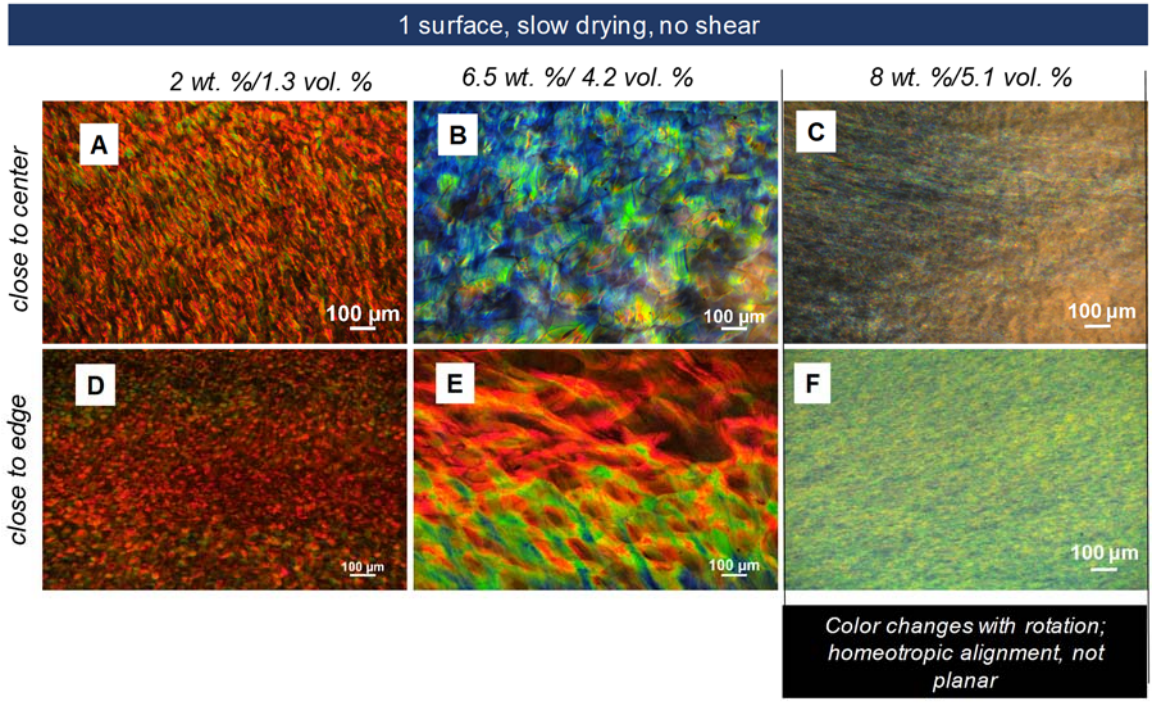

Figure S4. Cross-polarized reflected microscopic images showing CNC films made from isotropic (2 wt. %), biphasic (6.5 wt. %), and liquid crystalline (8 wt. %) using no coverslip, no shear, and humid environment drying. A), B), C) close to the center and D), E), F) close to the edge of the films.

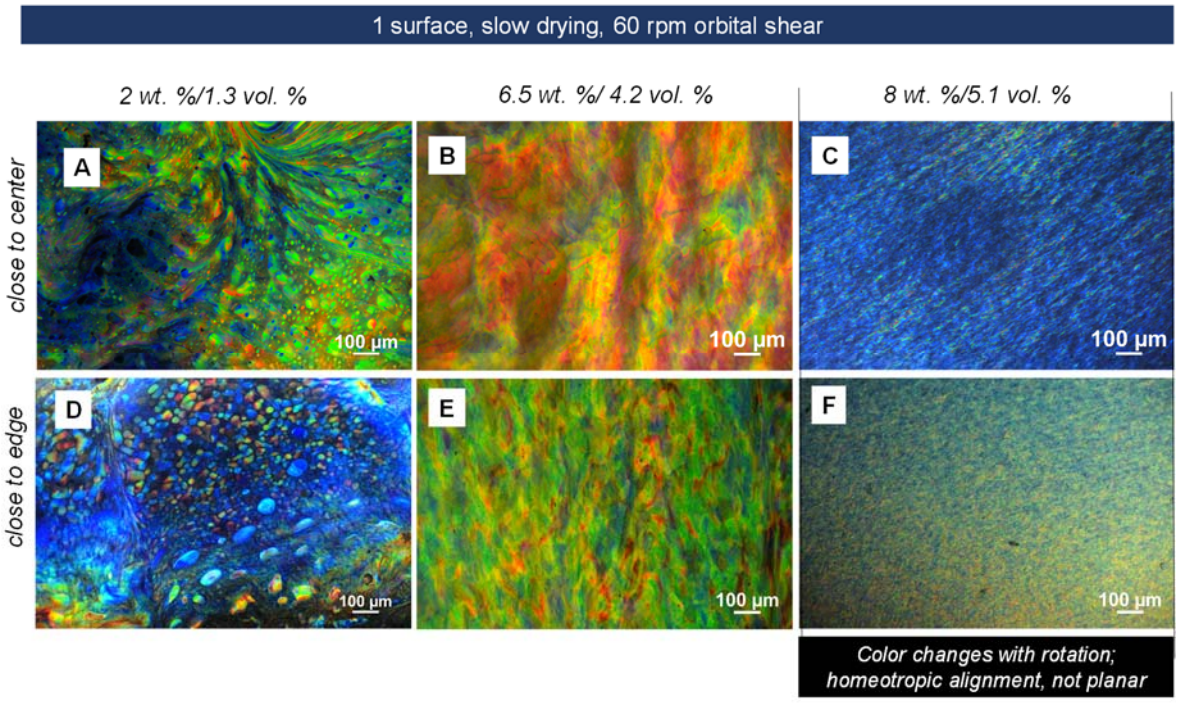

Figure S5. Cross-polarized reflected microscopic images showing CNC films made from isotropic (2 wt. %), biphasic (6.5 wt. %), and liquid crystalline (8 wt. %) using no coverslip, 60 rpm shear, and humid environment drying. A), B), C) close to the center and D), E), F) close to the edge of the films.

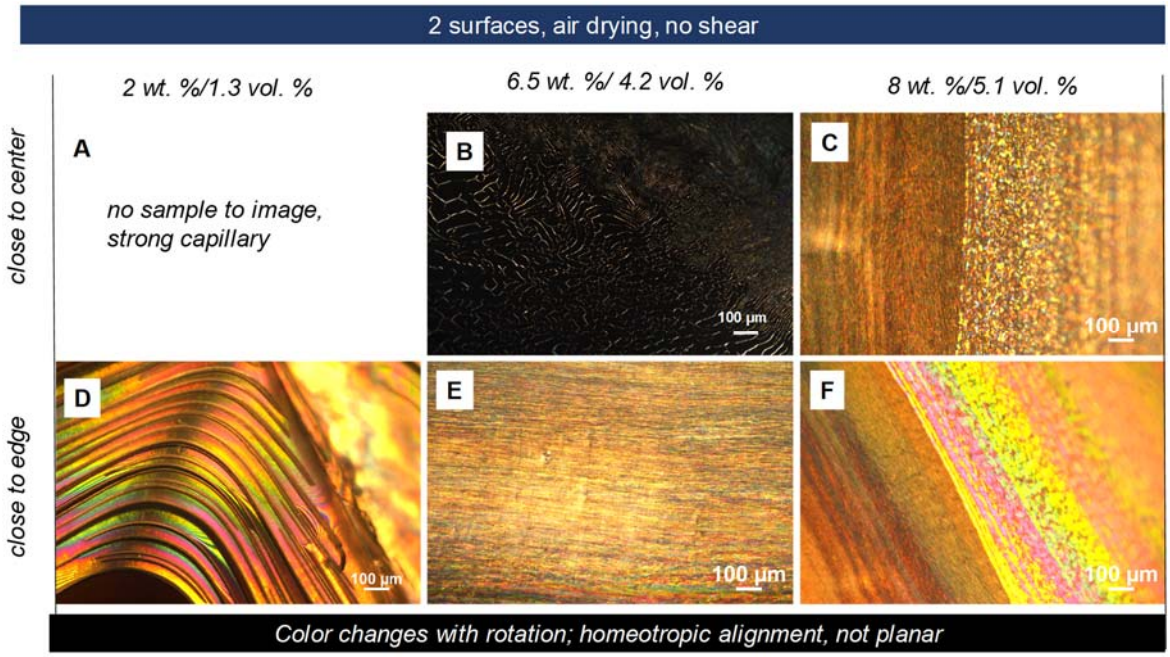

Figure S6. Cross-polarized reflected microscopic images showing CNC films made from isotropic (2 wt. %), biphasic (6.5 wt. %), and liquid crystalline (8 wt. %) using coverslip, no shear, and air drying. A), B), C) close to the center and D), E), F) close to the edge of the films.

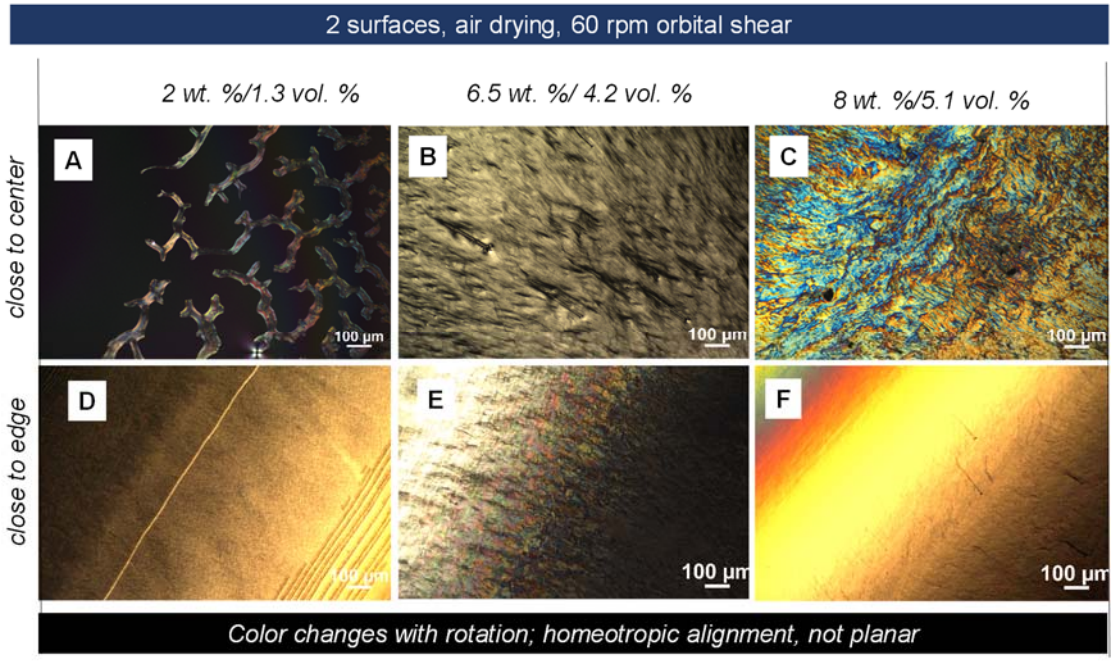

Figure S7. Cross-polarized reflected microscopic images showing CNC films made from isotropic (2 wt. %), biphasic (6.5 wt. %), and liquid crystalline (8 wt. %) using coverslip, 60 rpm shear, and air drying. A), B), C) close to the center and D), E), F) close to the edge of the films.

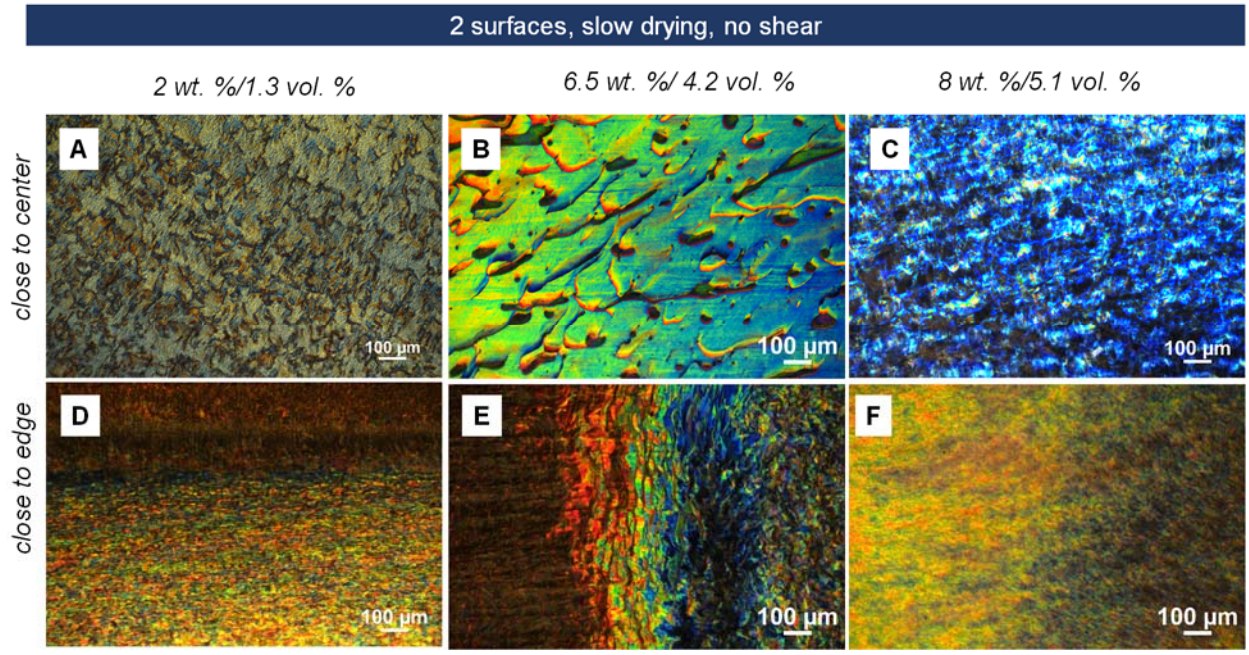

Figure S8. Cross-polarized reflected microscopic images showing CNC films made from isotropic (2 wt. %), biphasic (6.5 wt. %), and liquid crystalline (8 wt. %) using coverslip, no shear, and humid environment drying. A), B), C) close to the center and D), E), F) close to the edge of the films.

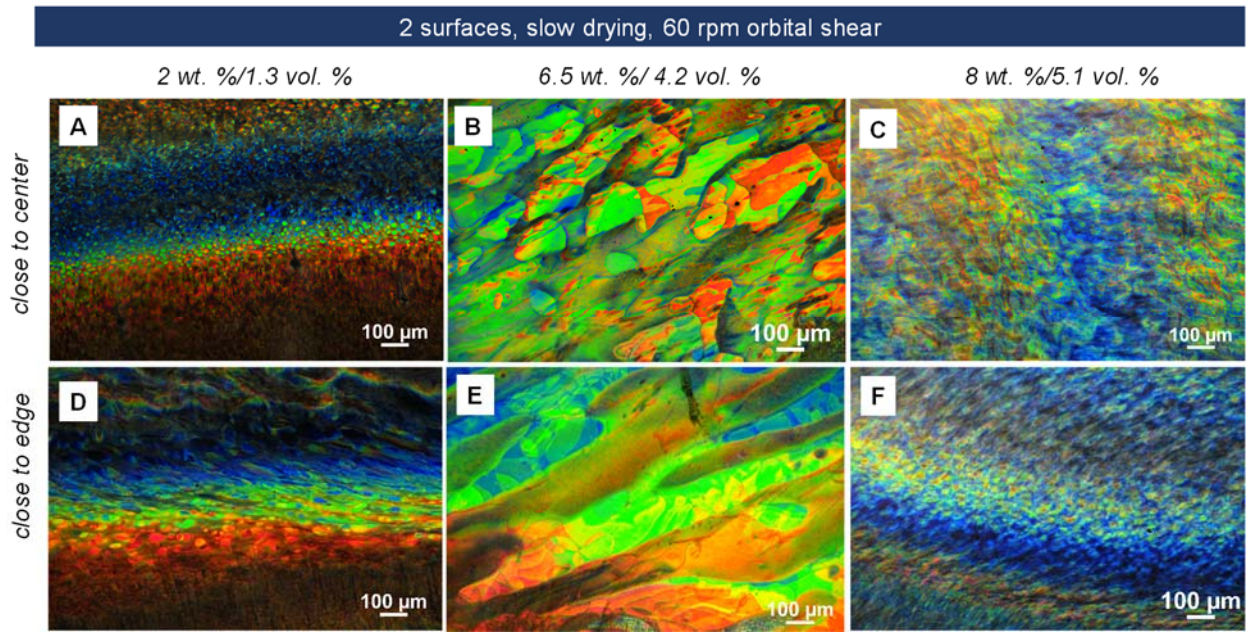

Figure S9. Cross-polarized reflected microscopic images showing CNC films made from isotropic (2 wt. %), biphasic (6.5 wt. %), and liquid crystalline (8 wt. %) using a coverslip, 60 rpm shear, and humid environment drying. A), B), C) close to the center and D), E), F) close to the edge of the films.

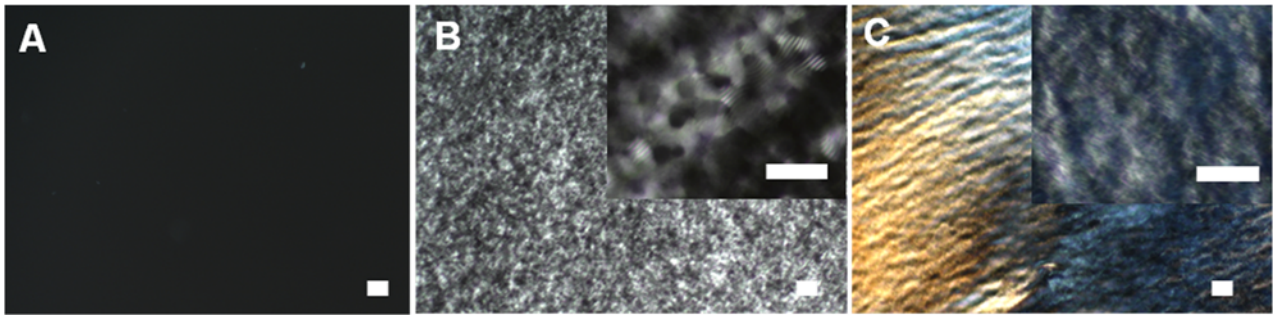

Figure S10. Cross-polarized transmitted light micrographs showing (A) 2.0 wt. %/1.3 vol. % (isotropic), (B) 6.5 wt. %/4.2 vol. % (biphasic), and (C) 8.0 wt. %/5.1 vol. % (liquid crystalline) dispersions of CNC. Scale bars are 50 μm.

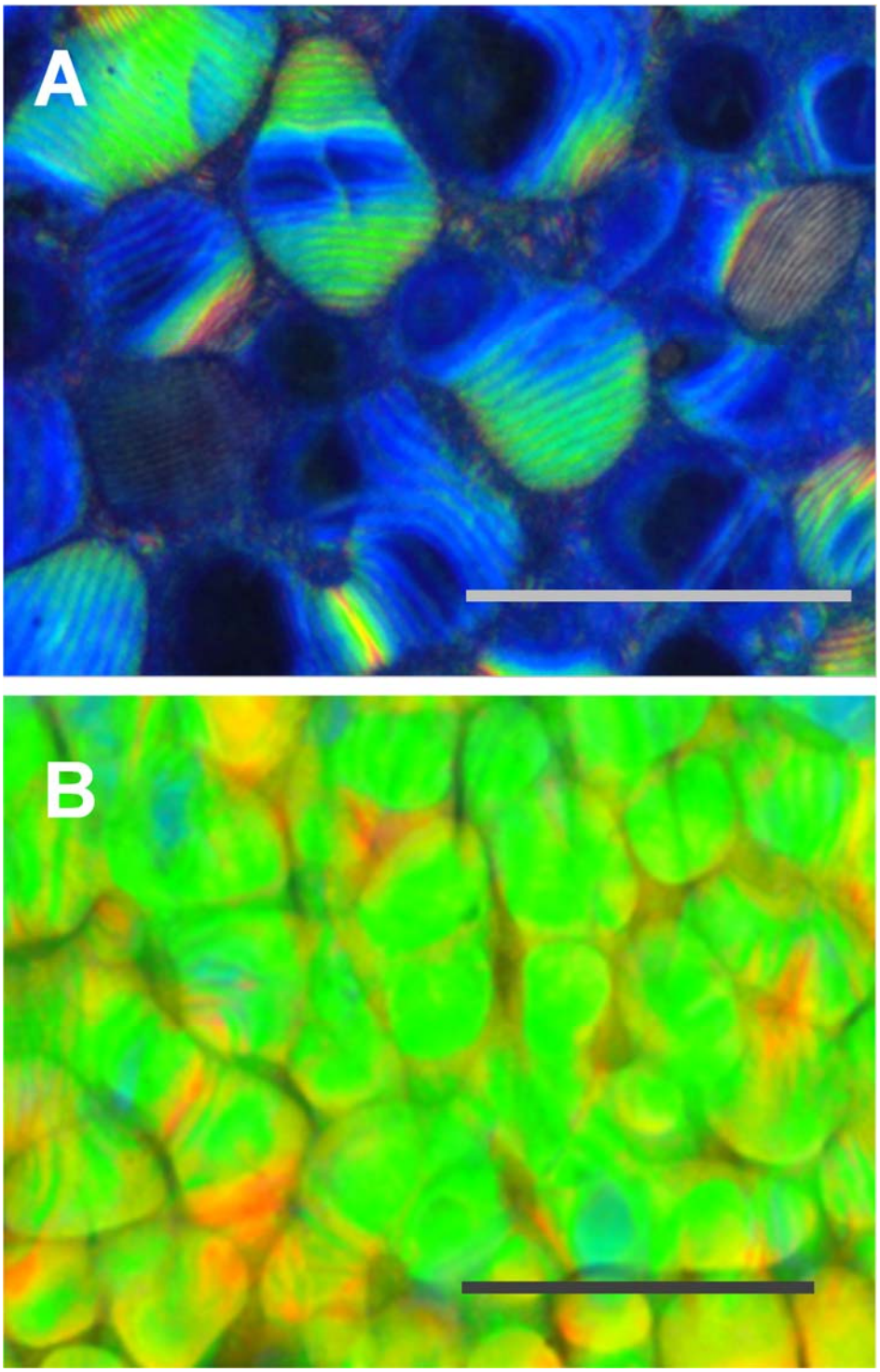

Figure S11. Enlarged versions of Figure 5. Cross-polarized reflected micrographs showing the effect of surface anchoring on planar orientation, CNC film dried in water vapor saturated environment assisted by orbital shear with a cover slip (A) off and (B) on during drying. Scale bars are 100 μm.

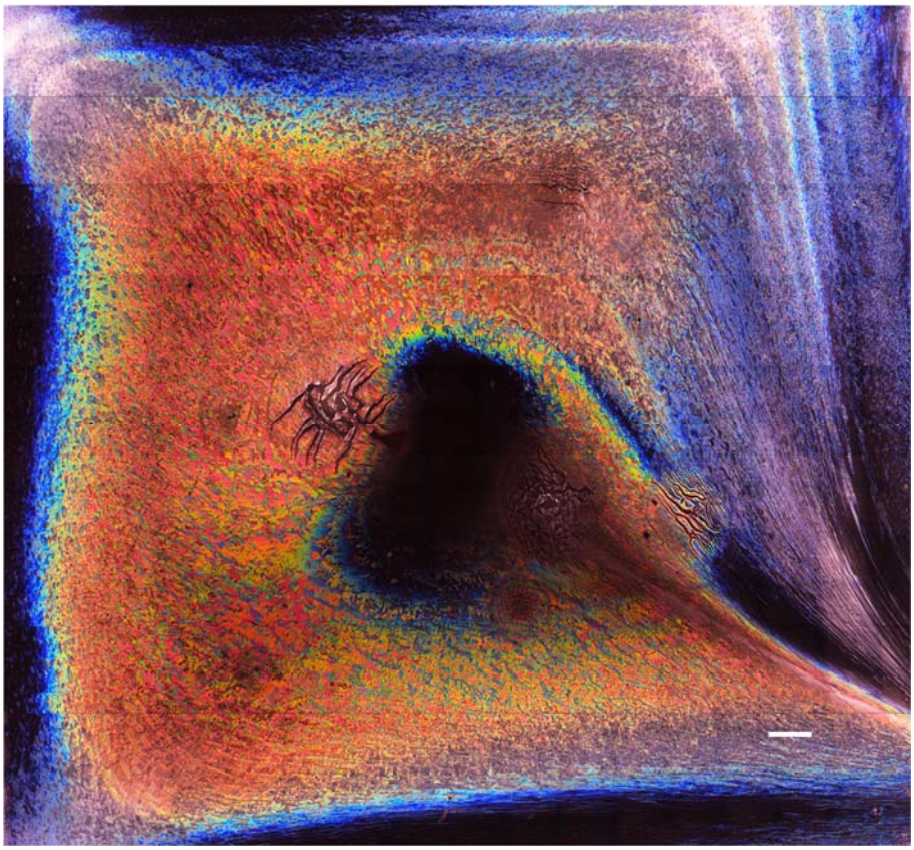

Figure S12. Cross-polarized reflected light microscopic stitched image of CNC film (using 6.5 wt. % CNC dispersion fabricated using surface anchoring, orbital shear, and water vapor saturated environment). Scale bar is 1 mm.

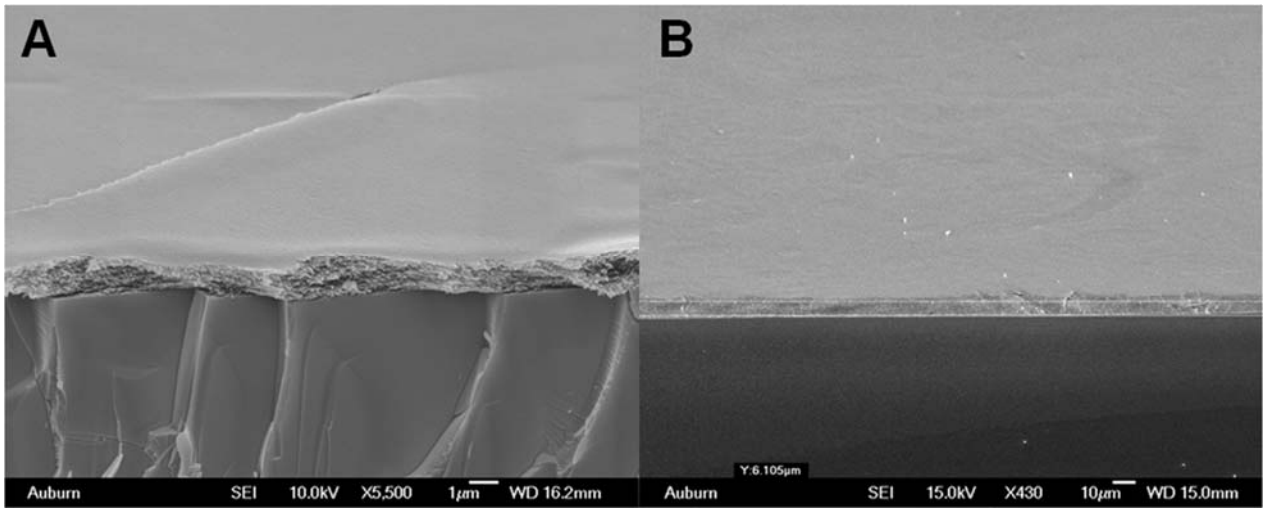

Figure S13. Scanning electron micrographs showing planar film thicknesses, (A) close to film center, scale bar and thickness approximately 1 μm (B) close to film edge. Scale bar and thickness approximately 10 μm.

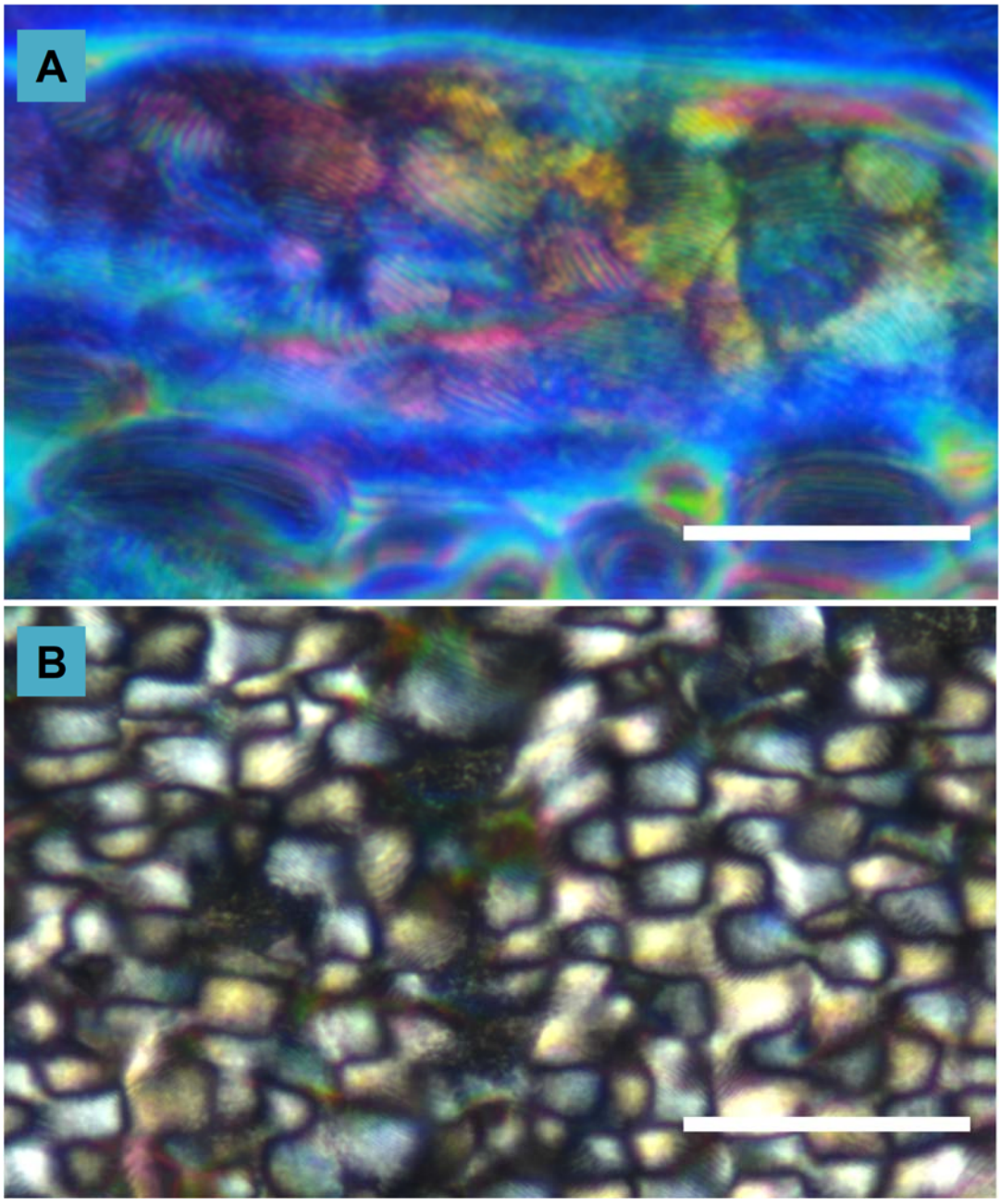

Figure S14. Cross-polarized (A) reflected and (B) transmitted light microscopic images showing focal conic and homeotropic texture in region 3R of Figure 7. Scale bars are 100 μm.

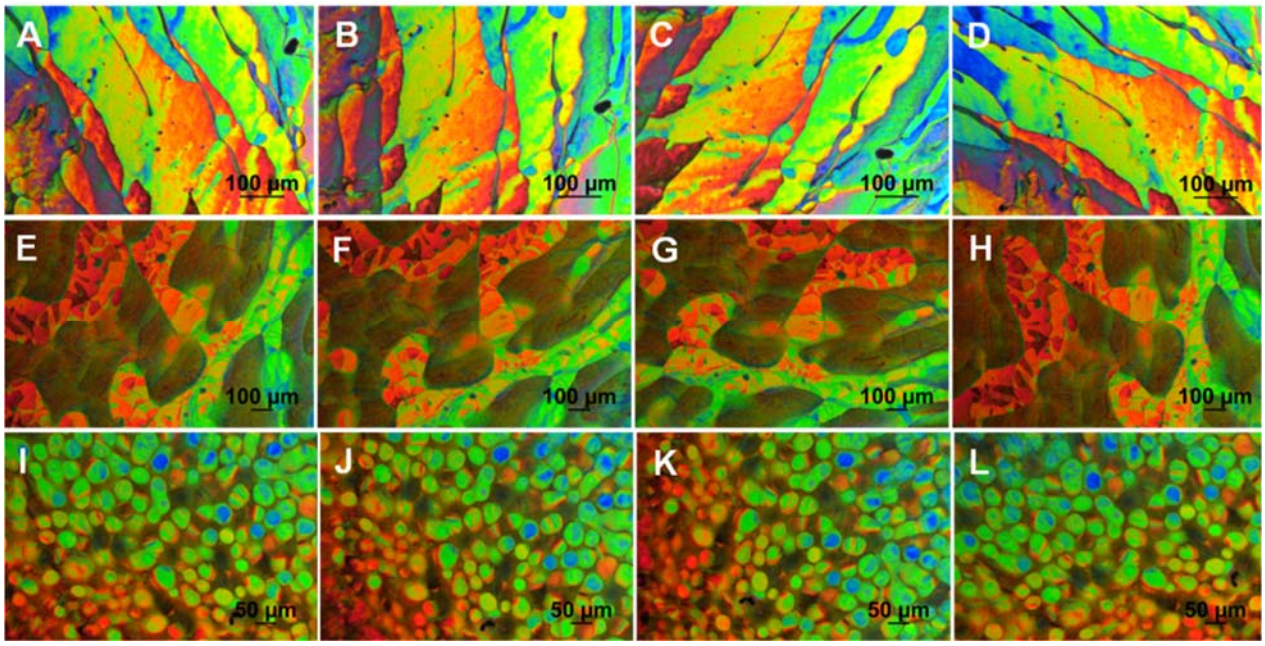

Figure S15. Cross-polarized reflected light micrographs showing no change of planar domains colors (no birefringence associated with homeotropic optical axis to the film is present) upon stage rotation (A) 0º, (B) 30º, (C) 60º, and (D) 90º for domains from Region 1 (using 6.5 wt. % dispersion), (E) 0º, (F) 30º, (G) 60º, and (H) 90º for domains from Region 3 (using 6.5 wt. % dispersion), and (I) 0º, (J) 30º, (K) 60º, and (L) 90º for domains found using 2 wt. % dispersion. Scale bars are 100 µm in A – H and 50 µm in I – L.

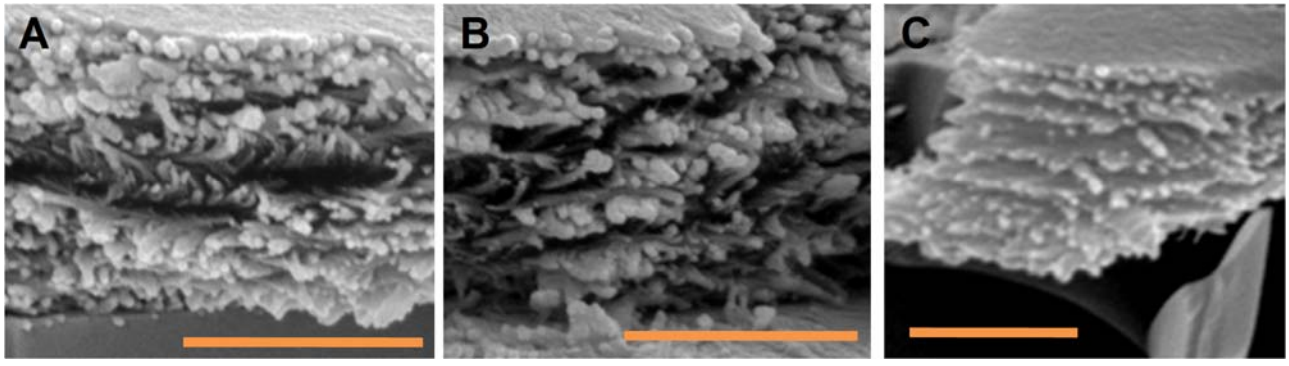

Figure S16. SEM for pitch calculation in Table 1 for (A) blue, (B) green, and (C) orange domains. Scale bars are 1 µm.

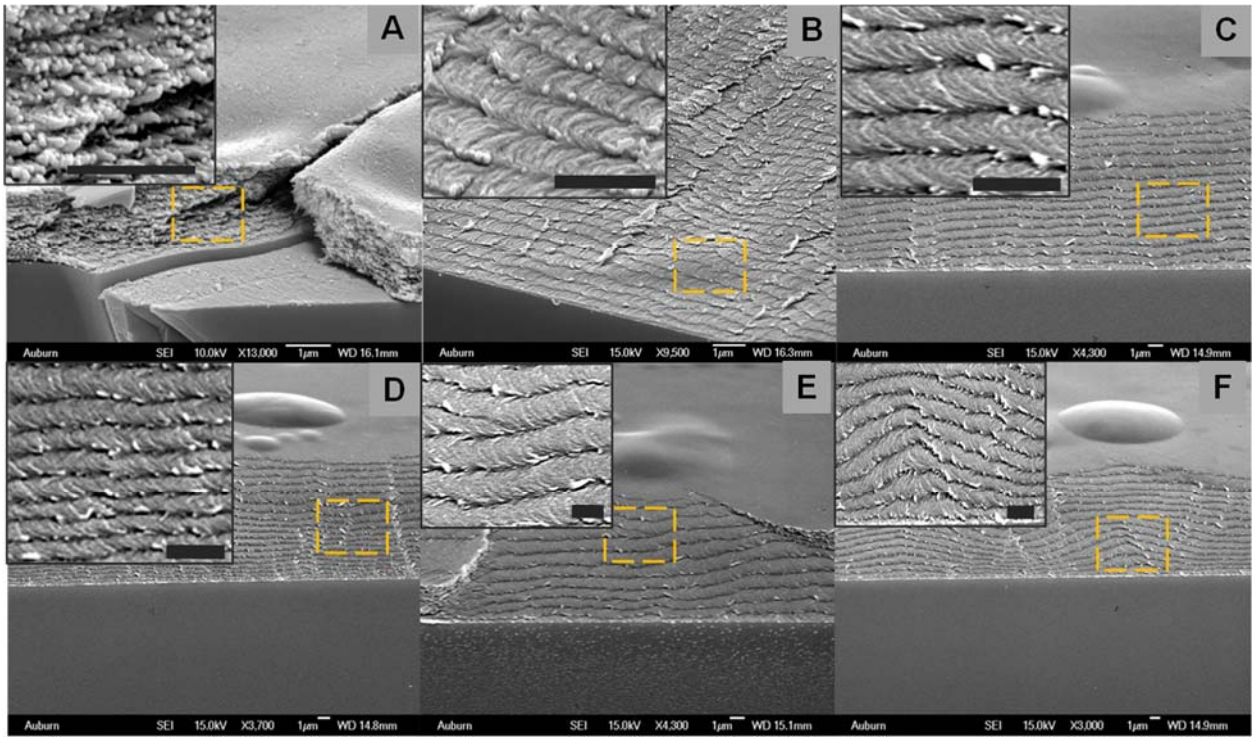

Figure S17. Enlarged version of Figure 10. Scanning electron microscope (SEM) images of cross-sections of CNC films showing (A) chiral nematic half-pitch segments viewed at 90° cross-section, (B) uniform parallel arc-like morphology of planar ordering viewed at oblique cross-section, (C) constant pitch and (D) spatially varying pitch within a planar domain, (E) line defect due to change of the number of chiral nematic half-pitch, and (F) tilted domains next to planar ones. The dome-shaped topography on the surface of the film is attributed to electron beam damage. Scale bars are 1 μm.